Journal of Sound and Vibration (1999) **228**(4), 731–760
Article No. jsvi.1999.2444, available online at http://www.idealibrary.com on IDEAL®

VIBRATION CONTROL OF SHEAR DEFORMABLE LAMINATED PLATES—MODELING IMPLICATIONS

MIN-YUNG CHANG

Mechanical Engineering Department, National Chung-Hsing University, Taichung, Taiwan 40227, *R.O.C.*

AND

LIVIU LIBRESCU

Engineering Science and Mechanics Department, Virginia Polytechnic and State University, Blacksburg, VA 24061, *U.S.A.*

(*Received* 9 *September* 1996, *and in final form* 27 *May* 1999)

A modal control approach is applied to control the vibration of homogeneous and laminated plates. The controller is designed using the linear optimal control theory. The performance of the controller designed according to a structural model of the plant based on the classical plate theory is evaluated and compared with that derived in the context of a higher order plate theory. It is found that the use of the classical plate model in the design of vibration control systems could lead to erroneous conclusions concerning the performance of the actual controlled system. The strong influence played by transverse shear deformation and lamination on the controlled system is clearly demonstrated and pertinent conclusions are outlined.

1. INTRODUCTION

Suppression of vibration via feedback control constitutes a topic of high practical importance in the design of the structural systems of advanced technology of today and tomorrow. Since the vibration of structural components can jeopardize their operational precision and precipitate their failure by fatigue, one should find appropriate ways to inhibit the oscillatory motion or at least to confine it.

Active control is an effective method to reach such a goal. The increasing interest in the application of such a methodology is certainly due to higher precision and/or stability requirements of many flexible structural systems in current times and the degree of maturity of existing feedback control approaches. For a list of references emphasizing the efforts and achievements in this area, the reader is referred to the monograph [1].

However, in spite of the tremendous work done so for in this area, few studies have been devoted to an assessment of the implications of transverse shear flexibility on vibration control of structures made from advanced composite

0022–460X/99/490731 + 30 $30.00/0

materials. In this paper, we intend to illustrate the importance of this effect on the control of homogeneous as well as laminated plates. However, before going further into the study of this problem, we should refer to the works [2, 3], where a mathematical treatment of the active control of thin plates was developed, as well as papers [4–6], where various problems related with the active control of flat plates have been presented.

As has been conclusively shown [7–9], the classical lamination theory based upon the adoption of the Kirchhoff hypothesis proves to be inadequate in many important instances. This is especially true whenever the constituent materials feature large flexibility in transverse shear and/or when the structure does not fulfill the thinness requirement imposed by the adoption of the Kirchhoff hypothesis. In such cases, in order to get reliable response predictions, refined structural models incorporating transverse shear and higher order effects have to be used.

In order to illustrate the limits of the applicability of the Kirchhoffean plate model on the design of the controller, the results obtained will be compared with the ones obtained in the context of a higher order plate theory developed in references [7, 8]. The latter model incorporates a number of non-classical structural effects such as transverse shear and normal stress, and fulfills the traction-free boundary conditions on the external bounding planes of the plate. In the context of the classical plate model, these effects are ignored.

Comparisons of the closed-loop response predictions obtained in the context of the two structural models will provide a measure of the influence of the modelling errors induced by the neglect of the above-mentioned non-classical effects. For the sake of the completeness, two modal control methodologies, namely the independent modal-space control (IMSC) and coupled modal-space control (CMC) [1, 10], are used for the purpose of controlling the vibration of laminated plates. The feedback control law is designed by using the linear optimal control theory [11]. As regards the performance index chosen to be minimized, it consists of an integral of the sum of the weighted vibration and control energies.

2. GOVERNING EQUATIONS

Consider the case of plates symmetrically laminated of $2m + 1$ laminae of uniform thickness. The mid-plane σ of the central layer (which coincides with the mid-plane of the entire laminate) is referred to an orthogonal system of co-ordinates (x, y), the z-axis being normal to σ. One assumes that the materials of the constituent layers feature transversely isotropic properties, the plane of isotropy in each material layer being parallel at each point to the mid-plane of the structure. The selection of this material for the present analysis is motivated by the following facts: (i) due to its special thermo-mechanical characteristics this material (known as pyrolitic graphite) is likely to become an excellent candidate for use in structural space applications, and (ii) it enables one to emphasize in a convenient and general way, via parametric studies, the implications on vibration control of transverse shear flexibility characteristics.

In light of the higher order theory (HOT) developed in reference [8], the displacement field associated with the bending problem assumes the form

$$V_\alpha(x, y, z, t) = z\beta_\alpha(x, y, t) + z^3\psi_\alpha(x, y, t), \quad \alpha = 1, 2, \tag{1a}$$

$$V_3(x, y, z, t) = w(x, y, t). \tag{1b}$$

In equations (1), V_α and V_3 denote, respectively, the tangential and transverse displacement components of the 3-D medium of the plate, $\beta_\alpha(\equiv\beta_\alpha(x, y, t))$ and $\psi_\alpha(\equiv\psi_\alpha(x, y, t))$ are 2-D displacement measures (see e.g. reference [8]) while t denotes the time. Following the developments carried out in references [7, 8], in the absence of rotatory inertia effects the equations governing the transverse bending motion can be expressed in a decoupled form in terms of the transverse deflection $w(x, y, t)$ and a transverse shear potential function $\Phi(\equiv\Phi(x, y, t))$ as

$$\begin{aligned} &D(w_{,xxxx} + 2w_{,xxyy} + w_{,yyyy}) - p + H_1(p_{,xx} + p_{,yy}) + M_0 w_{,tt} - K(w_{,xxtt} + w_{,yytt}) \\ &\quad - [(m_{1,y} + m_{2,x}) - H_2(m_{1,xxy} + m_{1,yyy} + m_{2,xxx} + m_{2,xyy})] = 0 \end{aligned} \tag{2a}$$

and

$$\Phi - \frac{C}{S}(\Phi_{,xx} + \Phi_{,yy}) = 0. \tag{2b}$$

In these equations the comma denotes the partial differentiation with respect to the indicated variables. Also p denotes the transverse load intensity, m_1 and m_2 represent the external moment intensities with their axes being parallel to the x-axis and y-axis, respectively, while the expressions of the mass and rigidity quantities appearing in these equations are displayed in Appendix B.

In the case of single-layered transversely isotropic plates, equations (2) can be modified as

$$\begin{aligned} &\frac{Eh^3}{12(1-\mu^2)}(w_{,xxxx} + 2w_{,xxyy} + w_{,yyyy}) - \left\{p - \frac{h^2}{10(1-\mu)}\left[\frac{E}{(1+\mu)G'} - \delta_A\frac{\mu' E}{E'}\right]\right. \\ &\left.(p_{,xx} + p_{,yy})\right\} - \left\{(m_{1,y} + m_{2,x}) - \frac{h^2}{30(1-\mu)}\left[\frac{E}{2(1+\mu)G} - \delta_A\frac{\mu E}{E}\right]\right. \\ &\left.(m_{1,xxy} + m_{1,yyy} + m_{2,xxx} + m_{2,xyy})\right\} + \rho h w_{,tt} - \frac{\rho h^3}{10}\left[\frac{E}{(1-\mu^2)G'} - \delta_A\frac{\mu' E}{6(1-\mu)G'}\right] \\ &(w_{,xxtt} + w_{,yytt}) = 0, \end{aligned} \tag{3a}$$

$$\Phi - \frac{h^2}{10}\frac{G}{G'}(\Phi_{,xx} + \Phi_{,yy}) = 0. \tag{3b}$$

In spite of the fact that the governing equations shown above are uncoupled, the boundary value problem remains coupled through the three boundaries at each

prescribed edge of the plate. In these equations as well as in the stiffness quantities given in Appendix B, E, $G(\equiv E/[2(1+\mu)])$, μ and E', G', μ' denote the Young's modulus, shear modulus and the Poisson ratio associated with the plane of isotropy and with the planes normal to the plane of isotropy respectively.

In order to incorporate the effect of constant edge loads, it can readily be shown that this can formally be done by replacing $p(\equiv p(x, y, t))$ by $p + T_x w_{,xx} + T_y w_{,yy}$, where T_x and T_y denote the in-plane edge loads parallel to the x- and y-axis, respectively, considered positive in tension.

Upon defining dimensionless quantities indicated by an overbar whose definitions are listed in Appendix C, the dimensionless counterparts of governing equations (2) become

$$\begin{aligned}\bar{B}\bar{w}_{,\overline{tt}} - \bar{C}_1\bar{w}_{,\overline{xxtt}} - \bar{C}_2\bar{w}_{,\overline{yytt}} - (\bar{T}_1\bar{w}_{,\overline{xx}} + \bar{T}_2\bar{w}_{,\overline{yy}}) + (\bar{D}_1 + \bar{T}_1\bar{F}_1)\bar{w}_{,\overline{xxxx}} \\ + (2 + \bar{T}_1\bar{F}_2 + \bar{T}_2\bar{F}_1)\bar{w}_{,\overline{xxyy}} + (\bar{D}_2 + \bar{T}_2\bar{F}_2)\bar{w}_{,\overline{yyyy}} = \bar{p}(\bar{F}_1\bar{p}_{,\overline{xx}} + \bar{F}_2\bar{p}_{,\overline{yy}}) \\ + (\bar{m}_{1,\bar{y}} + \bar{m}_{2,\bar{x}}) - [\bar{F}_{11}(\bar{m}_{2,\overline{xxx}} + \bar{m}_{1,\overline{xxy}}) + \bar{F}_{12}(\bar{m}_{2,\overline{xyy}} + \bar{m}_{1,\overline{yyy}})],\end{aligned} \tag{4a}$$

$$\bar{\Phi} - \bar{R}(\ell_R\bar{\Phi}_{,\overline{xx}} + \bar{\Phi}_{,\overline{yy}}) = 0. \tag{4b}$$

For the sake of simplification, henceforth the overbars associated with the dimensionless quantities are removed. Next, as a prerequisite to the study of the control problem, the eigensolutions and the dynamic response of the uncontrolled systems consisting of a simply supported laminated plate subjected to external loads, are addressed.

3. FREQUENCY AND DYNAMIC RESPONSE OF THE UNCONTROLLED SYSTEM

The study concerns rectangular ($\ell_1 \times \ell_2$) plates simply supported all around the contour. As was shown in reference [12], for simply supported panels the solution of equation (4b) representing the boundary layer effect is zero-valued and the expression of w that satisfies the simply supported boundary conditions can be expressed as

$$w(x, y, t) = \sum_{m,n=1}^{\infty} e^{i\Omega_{mn}t}(t)\sin m\pi x \sin n\pi y. \tag{5}$$

Consistent with this, the eigenfrequencies can be shown to be

$$\Omega_{mn}^2 = Q_3/Q_4, \tag{6a}$$

where

$$\begin{aligned}Q_3 = T_1D_1(\alpha_m^2 + T_R\beta_n^2)l_R^2 + D_1(D_1 + T_1F_1\}l_R^2\alpha_m^4 \\ + D_1[2l_R^2 + T_1F_1(1 + l_R^2T_R)]\alpha_m^2\beta_n^2 + (l_R^2 + D_1T_1F_1T_R)\beta_n^4,\end{aligned} \tag{6b}$$

$$Q_4 = D_1[Bl_R^2 + C_1(\alpha_m^2l_R^2 + \beta_n^2)]. \tag{6c}$$

In addition, $\ell_R (\equiv \ell_2/\ell_1)$ denotes the plate aspect ratio, $T_R (\equiv T_2/T_1)$ is the tensile edge load ratio while $\alpha_m = m\pi$, $\beta_n = n\pi$.

Upon including the proportional viscous-type damping effect, the modal equations associated with equation (4a) can be shown to reduce to

$$\ddot{q}_{mn}(t) + 2\xi_{mn}\Omega_{mn}\dot{q}_{mn}(t) + \Omega_{mn}^2 q_{mn}(t) = f_{dmn}(t), \quad m, n = 1, 2, \ldots, \tag{7}$$

where ξ_{mn} is the damping ratio, Ω_{mn} is given by equations (6) and

$$f_{dmn}(t) = \frac{1}{N_{mn}} \int_0^1 \int_0^1 \phi_{mn} \{[p - (F_1 p_{,xx} + F_2 p_{,yy}) + (m_{1,y} + m_{2,x}) + (m_{1,y} + m_{2,x}) - [F_{11}(m_{2,xxx} + m_{1,xxy}) + F_{12}(m_{2,xyy} + m_{1,yyy})]\} \mathrm{d}x\, \mathrm{d}y \tag{8a}$$

in which

$$N_{mn} = B + C_1 \alpha_m^2 + C_2 \beta_n^2, \tag{8b}$$

$$\phi_{mn} = 2 \sin m\pi x \sin n\pi y \tag{8c}$$

denote the generalized mass and the normalized eigenfunctions respectively.

4. CONTROL SYSTEM DESIGN

Active control of flexible structures is typically implemented to control a few known elastic modes. A linear state feedback regulator and a state observer (or Kalman–Bucy filter) are usually designed to control the desired modes of vibration. Higher modes referred to as residual modes are generally ignored in the analysis. However, they may be excited by the controller and fed through the observer to cause a new destabilizing effect on the system. This is referred to as the spillover phenomenon, which, as was shown by Balas [13], constitutes a major issue in the control of large space structures.

However, in the present study the spillover problem will not be addressed. Instead, our attention will be directed towards the assessment of the modelling errors on the response of the structure that is actively controlled. The modelling errors considered here are those due to the difference between the nominal and the actual plants. In this work, the nominal plant is assumed to coincide with the structural model based upon the Kirchhoff theory, while the actual plant is that based on the structural model which in contrast to the previously mentioned one, does not ignore transverse shear and higher order effects. The basic aim of this study consists, therefore, in an assessment of the adequacy of the classical model of the laminated flat structures for control system design as well as, in the clarification of the effects, on controlled responses, of a number of important structural parameters.

Suppose that in addition to an external disturbance force intensity $p(x, y, t)$, a control force distribution, $p_c(x, y, t)$, and two control moment distributions, $m_{c1}(x, y, t)$ and $m_{c2}(x, y, t)$, are also applied to the plate. In the case of the existence of M_1 concentrated control forces and of M_2 and M_3 concentrated control moments with their applied axes parallel to the x- and y-axis, respectively, the control force and moment distributions assume the form

$$p_c(x, y, t) = \sum_{i=1}^{M_1} \tilde{a}_i \delta(x - x_i)\delta(y - y_i),$$

$$m_{c1}(x, y, t) = \sum_{j=1}^{M_2} \tilde{m}_{1j} \delta(x - x_j)\delta(y - y_j),$$

$$m_{c2}(x, y, t) = \sum_{k=1}^{M_3} \tilde{m}_{2k} \delta(x - x_k)\delta(y - y_k), \tag{9}$$

where $\delta(\ )$ denotes the Dirac generalized function, $\tilde{a}_i$ are the amplitudes of control forces, while $\tilde{m}_{1j}$ and $\tilde{m}_{2k}$ are the amplitudes of control moments.

In light of equation (9), letting p_c, m_{c1} and m_{c2} be in place of p, m_1 and m_2 in equation (8a), the expression of the modal control inputs can be found to be

$$f_{cmn}(t) = \sum_{i=1}^{M_1} b_{mni}^{(1)} \tilde{a}_i(t) + \sum_{j=1}^{M_2} b_{mnj}^{(2)} \tilde{m}_{1j}(t) + \sum_{k=1}^{M_3} b_{mnk}^{(3)} \tilde{m}_{2k}(t), \tag{10a}$$

where

$$b_{mni}^{(1)} = \frac{1}{N_{mn}} [\phi_{mn}^{i} - (F_1 \phi_{mn,xx}^{i} + F_2 \phi_{mn,yy}^{i})], \tag{10b}$$

$$b_{mnj}^{(2)} = \frac{1}{N_{mn}} [- \phi_{mn,y}^{j} + (F_{11} \phi_{mn,xxy}^{j} + F_{12} \phi_{mn,yyy}^{j})], \tag{10c}$$

$$b_{mnk}^{(3)} = \frac{1}{N_{mn}} [- \phi_{mn,x}^{k} + (F_{11} \phi_{mn,xxx}^{k} + F_{12} \phi_{mn,yyy}^{k})], \tag{10d}$$

Hence, the modal equations of plate including the control inputs can be expressed as

$$\ddot{q}_{mn}(t) + 2\xi_{mn}\Omega_{mn}\dot{q}_{mn}(t) + \Omega_{mn}^2 q_{mn}(t) = f_{cmn}(t) + f_{dmn}(t), \quad m, n = 1, 2, \ldots. \tag{11}$$

4.1. MODAL CONTROL FORMULATIONS

Two modal active control methodologies are implemented referred to as coupled modal control (CMC) and independent modal-space control (IMSC) [10]. Within

the CMC approach the first $r \times s$ controlled modal equations are written in state-space form as

$$\dot{\mathbf{u}}_N = \mathbf{A}_N \mathbf{u}_N + \mathbf{B}_N \mathbf{z} + \mathbf{f}_d, \tag{12a}$$

and

$$\mathbf{u}_N^{\mathrm{T}} = [q_{11}, \ldots, q_{rs}, \dot{q}_{11}, \ldots, \dot{q}_{rs}], \tag{12b}$$

$$\mathbf{z}^{\mathrm{T}} = [\tilde{a}_1, \ldots, \tilde{a}_{M_1}, \tilde{m}_{11}, \ldots, \tilde{m}_{1M_2}, \tilde{m}_{21}, \ldots, \tilde{m}_{2M_3}], \tag{12c}$$

$$\mathbf{f}_d^{\mathrm{T}} = [0, \ldots, 0, f_{d11}, \ldots, f_{drs}], \tag{12d}$$

$$\mathbf{A}_N = \begin{bmatrix} \mathbf{O} & \mathbf{I} \\ -\Lambda_n & -\Lambda_{\xi n} \end{bmatrix},$$

$$\Lambda_n = diag\{\Omega_{11}^2, \ldots, \Omega_{rs}^2\},$$

$$\Lambda_{\xi n} = diag\{2\xi_{11}\Omega_{11}, \ldots, 2\xi_{rs}\Omega_{rs}\} \tag{12e–g}$$

and

$$\mathbf{B}_N = \begin{bmatrix} \mathbf{O} & \mathbf{O} & \mathbf{O} \\ \mathbf{B}_{n1} & \mathbf{B}_{n2} & \mathbf{B}_{n3} \end{bmatrix},$$

$$B_{nk} = \begin{bmatrix} b_{111}^{(k)} & \cdots & b_{1sM_k}^{(k)} \\ \vdots & \ddots & \vdots \\ b_{r11}^{(k)} & \cdots & b_{rsM_k}^{(k)} \end{bmatrix}, \quad k = 1, 2, 3 \tag{12h, i}$$

in which $\mathbf{O}$ and $\mathbf{I}$ denote the zero and identity matrices, $diag\{\ \}$ represents the diagonal matrix. Then, by selecting an appropriate control theory, a control law is designed where the feedback input vector $\mathbf{z}$ is expressed in terms of the state vector $\mathbf{u}_N$.

Within the IMSC, and in contrast to the CMC, one is able to design a controller for each mode to be controlled independently. One of the advantages of using the IMSC method is that the numerical work of designing the controller is less involved than in the CMC approach. The feedback gain generally can be obtained in closed form. This implies that less computation time is required and real-time implementation of the control algorithm is possible even for a system of relatively high order. In this approach, modal control inputs instead of physical control inputs are being designed. The actual control inputs are obtained in terms of modal control inputs by solving a set of simultaneously linear algebraic equations. The solution is exact if the number of control actuators is the same as the number of modes being controlled. The performance of the control system certainly will degrade if the number of the control actuators is less than the number of the modes

that one wants to control. In this study, the number of actuators and controlled modes is assumed to be the same.

Using the IMSC approach, every controlled modal equation is expressed in state-variable form as

$$\dot{\mathbf{v}}_{ij} = \mathbf{A}_{ij}\mathbf{v}_{ij} + \mathbf{b}_c f_{cij} + \mathbf{b}_c f_{dij}, \quad i = 1, \ldots, r \text{ and } j = 1, \ldots, s, \tag{13a}$$

where

$$\mathbf{A}_{ij} = \begin{bmatrix} 0 & 1 \\ -\Omega_{ij}^2 & -2\xi_{ij}\Omega_{ij} \end{bmatrix}, \qquad \mathbf{v}_{ij} = \begin{bmatrix} q_{ij} \\ \dot{q}_{ij} \end{bmatrix}, \qquad \mathbf{b}_c = \begin{bmatrix} 0 \\ 1 \end{bmatrix} \tag{13b–d}$$

and f_{dij} and f_{cij} are given by equations (8) and (10) respectively. Although the uncontrolled modal equations, equations (7), are not coupled, their controlled counterparts, equations (11), may become coupled when the feedback control law is used as would be the case for CMC. However, from equations (13) one can see that controlled modal equations become uncoupled if one selects the modal feedback control, f_{cij}, to be a function depending only on its associated modal state $\mathbf{v}_{ij}$, i.e., $f_{cij} = f_{cij}(\mathbf{v}_{ij})$. As a result, the controlled modal equations become uncoupled and the controller can be designed for each mode to be controlled independently. Moreover, due to the fact that the order of the controlled modal equation is low, one can design the controller in an easier way. Once the modal control inputs are obtained, the physical control inputs can be determined from equations (10).

4.2. LINEAR OPTIMAL REGULATOR

In the context of the present approaches the optimal control theory is adopted to design the control law and full states feedback is assumed. Since the purpose of the control of the structure here is to suppress its vibration, one may formulate the whole problem as a linear quadratic regulator with desired final states of system taken to be zero. In the following, the derivation of the optimal control law for a system subjected to external excitation loads is described.

For ease of illustration, without loss of generality, the state equations irrespective of the CMC or the IMSC approach, for the moment, will be assumed to be represented by

$$\dot{\mathbf{u}}(t) = \mathbf{A}\mathbf{u}(t) + \mathbf{B}\mathbf{z}(t) + \mathbf{f}_d(t). \tag{14}$$

The cost function (also known as the performance index) J, which is to be minimized, associated with the linear regulator problem is often chosen to have the following quadratic form:

$$J = \frac{1}{2}\mathbf{u}^{\mathrm{T}}(t_f)\mathbf{S}\mathbf{u}(t_f) + \frac{1}{2}\int_{t_0}^{t_f} (\mathbf{u}^{\mathrm{T}}(t)\mathbf{Q}\mathbf{u}(t) + \mathbf{z}^{\mathrm{T}}(t)\mathbf{R}\mathbf{z}(t)\,\mathrm{d}t, \tag{15}$$

where t_0 and t_f denote the initial and terminal time (both are assumed fixed) of the intended controlling period respectively. The **S** and **Q** represented the weighting matrices of terminal states and states respectively, and are constant, symmetric and non-negative definite. Matrix R denotes the weighting matrix of control inputs, and is constant, symmetric and positive definite. It is also assumed that the states and control inputs are not bounded and the terminal states are free. The optimal control inputs that minimize the cost given by equation (15) can be determined as follows:

First, define an augmented cost function that includes the state equations, equations (14), as constraints as

$$J_a = \frac{1}{2}\mathbf{u}^{\mathrm{T}}(t_f)\mathbf{S}\mathbf{u}(t_f) + \int_{t_0}^{t_f}\left\{\frac{1}{2}(\mathbf{u}^{\mathrm{T}}\mathbf{Q}\mathbf{u} + \mathbf{z}^{\mathrm{T}}\mathbf{R}\mathbf{z}) + \mathbf{I}_c^{\mathrm{T}}\ (\mathbf{A}\mathbf{u} + \mathbf{B}\mathbf{z} + \mathbf{f}_d - \dot{\mathbf{u}})\right\}\mathrm{d}t, \quad (16)$$

where $\mathbf{I}_c$ are the costates (also known as Lagrange's multipliers). The necessary conditions for the minimization of J_a (and hence of J) can be found by setting the first variation of equation (16) to zero. This yields

$$\dot{\mathbf{I}}_c = -\mathbf{Q}\mathbf{u} - \mathbf{A}^{\mathrm{T}}\mathbf{I}_c, \qquad \mathbf{R}\mathbf{z} + \mathbf{B}^{\mathrm{T}}\mathbf{I}_c = \mathbf{0}, \qquad \dot{\mathbf{u}} = \mathbf{A}\mathbf{u} + \mathbf{B}\mathbf{z} + \mathbf{f}_d \quad (17\text{a–c})$$

together with the following initial and terminal conditions of states:

$$\mathbf{u}(t_0) = \mathbf{u}_0, \qquad \mathbf{u}^{\mathrm{T}}(t_f)\mathbf{S} = \mathbf{I}_c^{\mathrm{T}}(t_f). \quad (18\text{a, b})$$

Equations (17a–c) can be written in matrix form as

$$\frac{\mathrm{d}}{\mathrm{d}t}\begin{bmatrix}\mathbf{u}\\ \mathbf{I}_c\end{bmatrix} = \begin{bmatrix}\mathbf{A} & -\mathbf{B}\mathbf{R}^{-1}\mathbf{B}^{\mathrm{T}}\\ -\mathbf{Q} & -\mathbf{A}^{\mathrm{T}}\end{bmatrix}\begin{bmatrix}\mathbf{u}\\ \mathbf{I}_c\end{bmatrix} + \begin{bmatrix}\mathbf{f}_d\\ \mathbf{0}\end{bmatrix}. \quad (19)$$

Denote Ψ to be the transition matrix of the above system and let it be partitioned according to the dimensions of **u** and $\mathbf{I}_c$ as follows:

$$\Psi = \begin{bmatrix}\psi_{11} & \psi_{12}\\ \psi_{21} & \psi_{22}\end{bmatrix}. \quad (20)$$

The solution of the system described by equation (19) then can be expressed for given terminal states as

$$\begin{bmatrix}\mathbf{u}(t)\\ \mathbf{I}_c(t)\end{bmatrix} = \begin{bmatrix}\psi_{11}(t-t_f) & \psi_{12}(t-t_f)\\ \psi_{21}(t-t_f) & \psi_{22}(t-t_f)\end{bmatrix}\begin{bmatrix}\mathbf{u}(t_f)\\ \mathbf{I}_c(t_f)\end{bmatrix} + \int_{t_f}^{t}\begin{bmatrix}\psi_{11}(t-\tau) & \psi_{12}(t-\tau)\\ \psi_{21}(t-\tau) & \psi_{22}(t-\tau)\end{bmatrix}\begin{bmatrix}\mathbf{f}_d\\ \mathbf{0}\end{bmatrix}\mathrm{d}\tau. \quad (21)$$

If taking into account of the terminal condition given by equation (18b), the costates $\mathbf{I}_c$ can be obtained from the above equations as

$$\mathbf{I}_c(t) = \mathbf{K}(t)\mathbf{u}(t) + \mathbf{d}(t), \tag{22a}$$

where

$$\mathbf{K}(t) = [\psi_{21}(t - t_f) + \psi_{22}(t - t_f)\mathbf{S}][\psi_{11}(t - t_f) + \psi_{12}(t - t_f)\mathbf{S}]^{-1}, \tag{22b}$$

$$\mathbf{d}(t) = -\mathbf{K}(t)\int_{t_f}^{t} \psi_{11}(t - \tau)\mathbf{f}(\tau)\,\mathrm{d}\tau + \int_{t_f}^{t} \psi_{22}(t - \tau)\mathbf{f}(\tau)\,\mathrm{d}\tau. \tag{22c}$$

In view of equation (22a), the optimal control inputs $\mathbf{z}$ determined from equation (17b) can be expressed as

$$\mathbf{z}(t) = \mathbf{z}_{cc}(t) + \mathbf{z}_{oc}(t). \tag{23}$$

Here $\mathbf{z}_{cc}$ and $\mathbf{z}_{oc}$ represent the closed-loop and open-loop control inputs, respectively, and

$$\mathbf{z}_{cc}(t) = -\mathbf{R}^{-1}\mathbf{B}^{\mathrm{T}}\mathbf{K}(t)\mathbf{u}(t), \tag{24a}$$

$$\mathbf{z}_{oc}(t) = -\mathbf{R}^{-1}\mathbf{B}^{\mathrm{T}}\mathbf{d}(t). \tag{24b}$$

The $\mathbf{K}(t)$ and $\mathbf{d}(t)$ in equations (24) remain to be determined. They can be shown to satisfy respectively the following equations:

$$\dot{\mathbf{K}}(t) = -\mathbf{Q} - \mathbf{A}^{\mathrm{T}}\mathbf{K}(t) - \mathbf{K}(t)\mathbf{A} + \mathbf{K}(t)\mathbf{B}\mathbf{R}^{-1}\mathbf{B}^{\mathrm{T}}\mathbf{K}(t) \tag{25a}$$

$$\dot{\mathbf{d}}(t) = -(\mathbf{A}^{\mathrm{T}} - \mathbf{K}(t)\mathbf{B}\mathbf{R}^{-1}\mathbf{B}^{\mathrm{T}})\mathbf{d}(t) - \mathbf{K}(t)\mathbf{f}_d(t) \tag{25b}$$

with the terminal conditions given by

$$\mathbf{K}(t_f) = \mathbf{S}, \qquad \mathbf{d}(t_f) = \mathbf{0}. \tag{25c–d}$$

If the external disturbance force is known exactly, one may solve equations (25) backwards in time to obtain the desired open-loop feedforward and closed-loop feedback time-varying variables, $\mathbf{d}(t)$ and $\mathbf{K}(t)$. However, if the nature of the external force is unknown or the force is applied to the structure unexpectedly and for a very short period of time, the above control approach may not work successfully. In such a case, one may consider using control inputs that only consist of the feedback term, i.e., $\mathbf{z}_{cc}$. By this method, the control inputs are not dependent upon the disturbance force, and still help reducing large peaks of vibration that may occur during the forcing period. After the disturbing force disappears, the vibration that remains can surely be eliminated very effectively by this feedback control action. In this paper, the latter control problem is investigated.

The control law can further be simplified by letting t_f approach infinity and $\mathbf{S} = 0$. It was shown by Kalman that under these conditions $\mathbf{K}(t)$ approaches a constant matrix $\mathbf{K}_c$ if the system is controllable and $\mathbf{A}$, $\mathbf{B}$, $\mathbf{R}$ and $\mathbf{Q}$ matrices are

constant [11]. The matrix $\mathbf{K}_c$ is determined from the following algebraic Riccati equation:

$$-\mathbf{K}_c\mathbf{A} - \mathbf{A}^{\mathrm{T}}\mathbf{K}_c - \mathbf{Q} + \mathbf{K}_c\mathbf{B}\mathbf{R}^{-1}\mathbf{B}^{\mathrm{T}}\mathbf{K}_c = \mathbf{0}. \tag{26}$$

The steady state linear optimal control inputs are then given by

$$\mathbf{z} = -\mathbf{R}^{-1}\mathbf{B}^{\mathrm{T}}\mathbf{K}_c\mathbf{u} \tag{27}$$

and the cost function J described by equation (15) reduces to (letting $t_0 = 0$)

$$J = \frac{1}{2}\int_0^{\infty} (\mathbf{u}^{\mathrm{T}}\mathbf{Q}\mathbf{u} + \mathbf{z}^{\mathrm{T}}\mathbf{R}\mathbf{z})\,\mathrm{d}t. \tag{28}$$

In view of equation (27), the system equation (14), can be put into the following form:

$$\dot{\mathbf{u}} = (\mathbf{A} - \mathbf{B}\mathbf{R}^{-1}\mathbf{B}^{\mathrm{T}}\mathbf{K}_c)\mathbf{u} + \mathbf{f}_d. \tag{29}$$

The dynamic responses of the controlled system can be obtained by solving the above equation.

It is worth mentioning here that although the condition $t_f \to \infty$ is used to obtain $\mathbf{K}_c$, in practice, the control objective can generally be achieved within a finite period of time. This is so because, for a preselected finite terminal time t_f, matrix $\mathbf{K}(t)$ obtained from equation (25a) will not vary with time until t approaches the neighborhood of t_f (see reference [11]). Hence, by a proper design of control inputs (through selections of weighting matrices in the Riccati equation), desired control results can be obtained much earlier than the selected t_f. It may, therefore, be justifiable to use the constant $\mathbf{K}_c$ instead of the time-varying $\mathbf{K}(t)$ when there is no strict constraint being imposed on the terminal time t_f.

Above some optimal control formulations relevant to vibration control problems studied here are derived. Next, the introduction of the control inputs described by equation (27) into the systems based on the CMC and IMSC formulations will be discussed separately in the following:

For CMC Formulation, we define a cost kernel C_T as

$$C_T = \tfrac{1}{2}(\mathbf{u}_N^{\mathrm{T}}\mathbf{Q}\mathbf{u}_N + \mathbf{z}^{\mathrm{T}}\mathbf{R}_c\mathbf{z}), \tag{30a}$$

where

$$\mathbf{Q} = \begin{bmatrix} \Lambda_1 & \mathbf{0} \\ \mathbf{0} & \Lambda_2 \end{bmatrix}, \qquad \Lambda_1 = diag\{q_{w11}\Omega_{11}^2, \ldots, q_{wrs}\Omega_{rs}^2\},$$

$$\Lambda_2 = diag\{q_{w11}, \ldots, q_{wrs}\}. \tag{30b–d}$$

When the state weighting matrix $\mathbf{Q}$ is chosen as that given by equations (30b–d), the first term in equation (30a) represents a sum of the weighted vibration energy of each mode to be controlled. According to equations (28) and (30a), the cost function

J can be expressed as

$$J = \frac{1}{2}\int_0^\infty C_T \, \mathrm{d}t. \tag{31}$$

A suitable $\mathbf{K}_c$ can be obtained by properly choosing the weighting matrices $\mathbf{Q}$ and $\mathbf{R}_c$ and solving an algebraic Riccati equation. The dynamical response of the optimally controlled system can then be found by solving the following equation:

$$\dot{\mathbf{u}}_N = \mathbf{A}_N^* \mathbf{u}_N + \mathbf{f}_d, \tag{32a}$$

where $\mathbf{A}_N^*$ is the closed-loop system matrix and

$$\mathbf{A}_N^* = \mathbf{A}_N - \mathbf{B}_N \mathbf{R}_c^{-1} \mathbf{B}_N^{\mathrm{T}} \mathbf{K}_c \tag{32b}$$

To obtain the solution of equations (32), the following integral formula of the linear system theory is used:

$$\mathbf{u}_N(t) = \mathbf{M}\mathrm{e}^{\mathbf{D}t}\mathbf{M}^{-1}\mathbf{u}_N(0) + \int_0^t \mathbf{M}\mathrm{e}^{\mathbf{D}(t-\tau)}\mathbf{M}^{-1}\mathbf{f}_d(\tau)\,\mathrm{d}\tau. \tag{33}$$

Here $\mathbf{M}$ represents the transformation matrix whose columns are the right eigenvectors of $\mathbf{A}_N^*$ and

$$\mathbf{D} = diag\{\lambda_1, \lambda_2, \ldots, \lambda_N\}, \tag{34}$$

where λ_i are the eigenvalues of $\mathbf{A}_N^*$, which are closed-loop poles. The expression of $\mathbf{D}$ implies that all the eigenvalues of $\mathbf{A}_N^*$ are distinct, which is assumed here. Let us partition matrices $\mathbf{M}$ and $\mathbf{M}^{-1}$as

$$\mathbf{M} = [\mathbf{m}_1, \mathbf{m}_2, \ldots, \mathbf{m}_N], \qquad \mathbf{M}^{-1} = [\mathbf{n}_1, \mathbf{n}_2, \ldots, \mathbf{n}_N]^{\mathrm{T}} \tag{35a, b}$$

and denote

$$\mathbf{m}_r\mathbf{n}_r^{\mathrm{T}} = \mathbf{S}_{Rr} + \mathrm{i}\mathbf{S}_{Ir}, \qquad \lambda_r = -\eta_r + \mathrm{i}\gamma_r. \tag{36a, b}$$

Here $\mathrm{i}(\equiv\sqrt{-1})$ denotes the imaginary unit. In view of equations (33–36), $\mathbf{u}_N$ can also be expressed as

$$\begin{aligned}\mathbf{u}_N(t) = \sum_{r=1}^{N} \Big\{ & \mathrm{e}^{-\eta_r t}(\mathbf{S}_{Rr}\cos\gamma_r t - \mathbf{S}_{Ir}\sin\gamma_r t)\mathbf{u}_N(0) \\ & + \mathbf{S}_{Rr}\int_0^t \mathrm{e}^{-\eta_r(t-\tau)}\cos\gamma_r(t-\tau)\mathbf{f}_d(\tau)\,\mathrm{d}\tau \\ & - \mathbf{S}_{Ir}\int_0^t \mathrm{e}^{-\eta_r(t-\tau)}\sin\gamma_r(t-\tau)\mathbf{f}_d(\tau)\,\mathrm{d}\tau \Big\}.\end{aligned} \tag{37}$$

In contrast to that of the CMC formulation, the cost kernel C_T based on the IMSC formulation is defined as

$$C_T = \tfrac{1}{2}(\mathbf{u}_N^{\mathrm{T}}\mathbf{Q}\mathbf{u}_N + \mathbf{f}^{\mathrm{T}}\mathbf{R}_I\mathbf{f}) \tag{38a}$$

or

$$C_T = \frac{1}{2}\sum_{i=1}^{r}\sum_{j=1}^{s}(\mathbf{v}_{ij}^{\mathrm{T}}\mathbf{Q}_{ij}\mathbf{v}_{ij} + r_{wij}f_{cij}), \tag{38b}$$

where

$$\mathbf{R}_I = diag\{r_{w11}, \ldots, r_{wrs}\}, \qquad \mathbf{f}_c = [f_{c11}, \ldots, f_{crs}]^{\mathrm{T}},$$

$$\mathbf{Q}_{ij} = q_{wij}\begin{bmatrix}\Omega_{ij} & 0\\ 0 & 1\end{bmatrix}. \tag{38c–e}$$

The cost function J is determined from equation (31), which in view of equation (38b) can be written as

$$J = \sum_{i=1}^{r}\sum_{j=1}^{s} J_{ij}, \tag{39a}$$

where

$$J_{ij} = \frac{1}{2}\int_0^{\infty}(\mathbf{v}_{ij}^{\mathrm{T}}\mathbf{Q}_{ij}\mathbf{v}_{ij} + r_{wij}f_{cij})\,\mathrm{d}t. \tag{39b}$$

Since f_{cij} is a function of only its own state $\mathbf{v}_{ij}$, all J_{ij} are independent. As a result, when J in equation (37a) is minimized, each J_{ij} should also be a minimum, and vice versa. Hence, using the IMSC approach, the control problem becomes finding an optimal modal control input f_{cij} for each system given in equations (13) such that every modal cost function J_{ij} given by equation (39b) is minimized. Because of the lower order of the systems (all are of second order), the solution of the algebraic Riccatti equation as well as the closed-loop poles can be obtained in closed form. The detail of these developments can be found in the references [1, 10].

After the optimal modal control inputs $\mathbf{f}_c$ are designed, in view of equations (11) the physical control inputs $\mathbf{z}$ can be determined by $\mathbf{f}_c = \mathbf{B}_n^*\mathbf{z}$ where $\mathbf{B}_n^* = [\mathbf{B}_{n1}\ \mathbf{B}_{n2}\ \mathbf{B}_{n3}]$ in which

$$\mathbf{B}_{nk} = \begin{bmatrix} b_{111}^{(k)} & \cdots & b_{11M_k} \\ \vdots & \ddots & \vdots \\ b_{rs1}^{(k)} & \cdots & b_{rsM_k}^{(k)} \end{bmatrix}, \quad k = 1, 2, 3. \tag{40}$$

The $\mathbf{z}$ found using the above relation are exact if the matrix $\mathbf{B}_n^*$ is square and non-singular. In other cases, a generalized inverse of $\mathbf{B}_n^*$ may be used.

It was shown in reference [10] that if the number of actuators and controlled modes are the same and if $\mathbf{R}_c = \mathbf{B}_n^{*\mathrm{T}}\mathbf{R}_I\mathbf{B}_n^*$, the cost kernels C_T (and hence the cost functions J) obtained using the CMC and IMSC approaches are identical. These

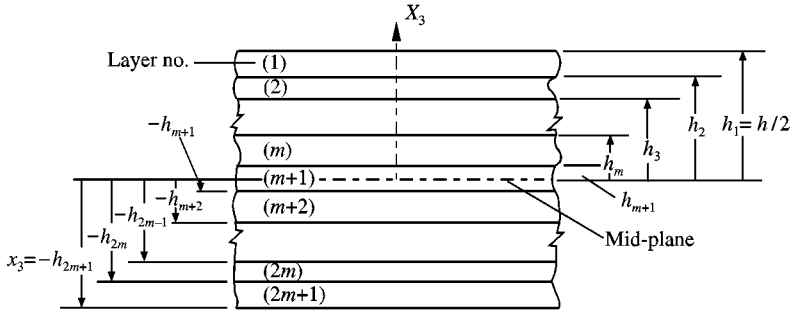

Figure 1. Cross-section of a symmetric laminated plate.

results are also used toward verification of the computer programs developed for the present analysis.

5. NUMERICAL ILLUSTRATIONS AND DISCUSSION OF RESULTS

The numerical illustrations are performed in the context of single and symmetrical three-layered flat panels.

For the three-layered panels (or laminates), the central layer is twice as thick as the outer face layers, implying the $h_{(1)}/h$ ($\equiv h_{(3)}/h$) $= 0{\cdot}5$ and $h_{(2)}/h = 0{\cdot}25$ (See Figure 1). Due to symmetry, the face layers are identical in their geometrical and material properties. Two types of three-layered panels, labelled as Laminates A and B, for the purpose of illustration are studied in this paper. They are defined as

Laminate A:

$$E_{(1)}/G'_{(1)}(\equiv E_{(3)}/G'_{(3)}) = 10, \qquad E_{(2)}/G'_{(2)} = 50, \qquad E_{(1)}/E'_{(1)}(\equiv E_{(3)}/E'_{(3)}) = 5,$$
$$E_{(2)}/E'_{(2)} = 5, \qquad E_{(1)}/E_{(2)} = 0{\cdot}2.$$

Laminate B:

$$E_{(1)}/G'_{(1)}(\equiv E_{(3)}/G'_{(3)}) = 50, \qquad E_{(2)}/G'_{(2)} = 10, \qquad E_{(1)}/E'_{(1)}(\equiv E_{(3)}/E'_{(3)}) = 5,$$
$$E_{(2)}/E'_{(2)} = 5, \qquad E_{(1)}/E_{(2)} = 5.$$

For simplicity, it is assumed that in both instances Poisson ratios and mass density of all layers are the same. In the numerical examples, $\mu_{(i)} = \mu'_{(i)} = 0{\cdot}25$ are considered.

The data characterizing Laminates A and B reveal that in the case of the former laminate, the face layers feature lower transverse shear flexibility than the core layer, (situation which is common to sandwich-type structures), whereas in the latter case, the opposite feature becomes apparent. The origin of the co-ordinates of the reference plane is chosen at the left corner of the rectangular plate. The plate is

assumed to be subjected to a harmonic concentrated load travelling at constant speed v along the straight line, $y = y_0$, parallel to the x-axis. Under these conditions p assumes the form

$$p(x, y, t) = \begin{cases} p_0\delta(x - vt)\delta(y - y_0)\cos\omega t & 0 \leqslant vt \leqslant 1, \\ 0, & vt \geqslant 1. \end{cases} \tag{41}$$

For the definition of the dimensionless quantities of the travelling load, see Appendix C. In the displayed numerical illustrations the transverse deflection of the center of the plate is represented and the co-ordinate y_0 is chosen to be 0·5. The time history of the deflection response is divided into two parts. The time interval with the moving load indicates the forced vibration, while the other indicates the free vibration as the moving load has already left the plate.

In numerical examples, there are totally nine vibration modes ($m, n = 1, 2, 3$) used in the controller design as well as in simulation, and the weighting parameters q_{wrs} are taken to be 1 and the same value of $r_{wrs}(\equiv r_w)$ are used for all the controlled modes.

There are two groups of actuators being considered in this paper. Among them, two types of torque actuators need to be differentiated. They are torque actuators that produce moments about an axis parallel to the x-axis and to the y-axis respectively. For ease of reference, they will be referred to as torque-I and torque-II actuators. Two groups of actuators selected are located at

Group 1:

Force actuators (0·5, 0·5), (0·35, 0·75), (0·65, 0·25),

Torque-I actuators (0·5, 0·1), (0·7, 0·9), (0·3, 0·2),

Torque-II actuators (0·1, 0·5), (0·9, 0·3), (0·2, 0·7).

Group 2:

Force actuators (0·5, 0·5), (0·35, 0·75), (0·65, 0·25),

Torque-I actuators (0·25, 0·25), (0·5, 0·8), (0·75, 0·25),

Torque-II actuators (0·2, 0·5), (0·8, 0·25), (0·8, 0·75).

Note that the numbers inside the parentheses are the dimensionless x and y representing the locations of the actuators.

In order to illustrate the significance of the plate theories adopted here, in Figure 2 there are compared the uncontrolled deflections predicted by HOT, FOT and CT of a plate of moderate thickness ($\ell_1/h = 10$). It is found that the results obtained from HOT and FOT are quite close, but CT greatly underestimates the deflection. It is worth mentioning here that for the case of single-layered plates, the contribution of higher order terms, which are considered in HOT, is equivalent to the incorporation of the shear correction factor of 5/6 in the FOT.

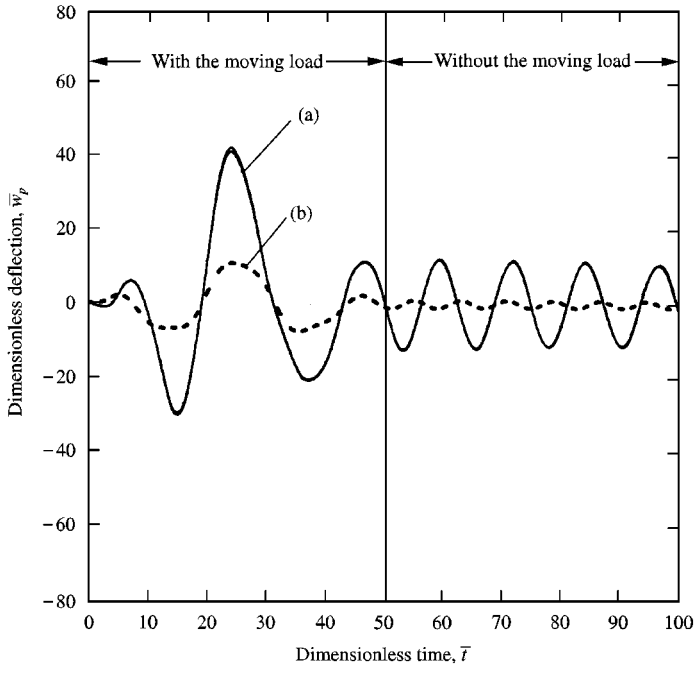

Figure 2. Uncontrolled dimensionless transverse deflections of a plate predicted by various plate models. $\ell_1/h = 10$, $\ell_R = 0{\cdot}75$, $\bar{\nu} = 0{\cdot}02$, $\bar{T}_1 = \bar{T}_2 = 0$, $\xi = 0{\cdot}005$, $\bar{\omega} = 0{\cdot}25$, (a) HOT ($E/G' = 50$, $E/E' = 5$) & FOT ($E/G' = 50$, $k^2 = 5/6$), (b) CT.

In Figure 3, controlled versus uncontrolled deflections of a plate using actuators of group 1 are shown. It is found that when the plate is modelled by CT, the controlled deflection of the plate during the forcing period (i.e., the travelling force is still acting on the plate) is greatly underestimated. This is evident when one compares the above controlled deflection with those of the plate with the actual plant modelled by either HOT or FOT. In Figure 4, the effect of E/G' ratio (which represents a degree of transverse shear rigidity) on the first force actuator of group 1 is shown. As the ratio increases, the deviation of the magnitude of the actuator's output from CT counterpart also increases. In Figure 5, the influence of E/G' ratios on the cost kernel C_T (which constitutes a measure of the vibration energy of structure and actuator's expenditure) is illustrated. In Figure 6, the influence of initial stresses on the controlled plate's deflection is demonstrated. It is shown that if the compressive in-plane stresses are present in the plate and are not taken into account in the controller's design, the controlled system will degrade further its performance.

From Figures 7–14, the uncontrolled and controlled dynamic responses of laminates A and B with the thickness ratio, ℓ_1/h, being 20 and 10 are studied. The uncontrolled deflections of laminates are compared in Figures 7 and 8. The results show that the deflection obtained from CT (which is the same for Laminates A and B) is much lower than those of HOT. Furthermore, one finds that the vibration amplitudes of laminates are still large even after the load has moved away from plate, and remain so for a long period time as the structural damping is light. In

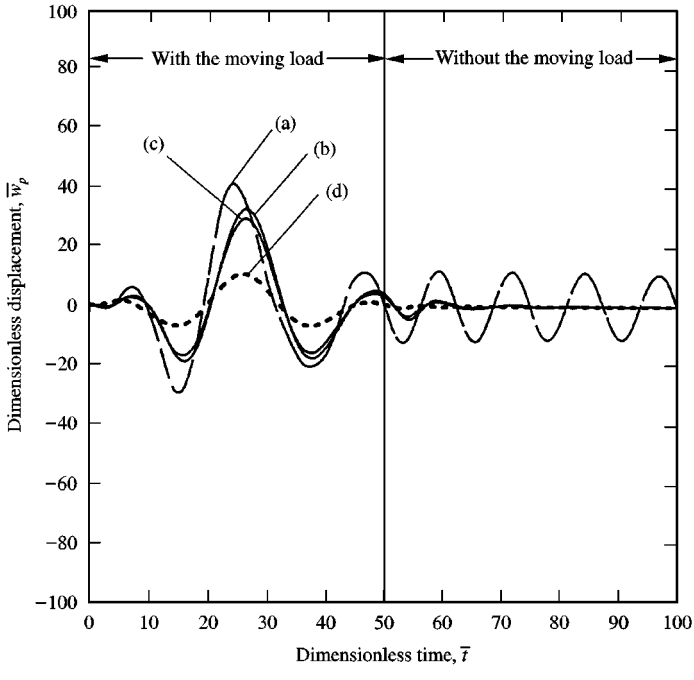

Figure 3. Controlled and uncontrolled dimensionless transverse deflections of a plate predicted by various plate models. CMC and IMSC, $\mathbf{R}_c = r_w \mathbf{B}_n^{*\mathrm{T}} \mathbf{B}_n^*$, $r_w = 10$, $q_w = 1$, nominal plant: CT. In the remaining all the input data and convention are common to the ones in Figure (2). (a) Uncontrolled (HOT), (b) actual plant: HOT, (c) actual plants: FOT, (d) actual plants: CT.

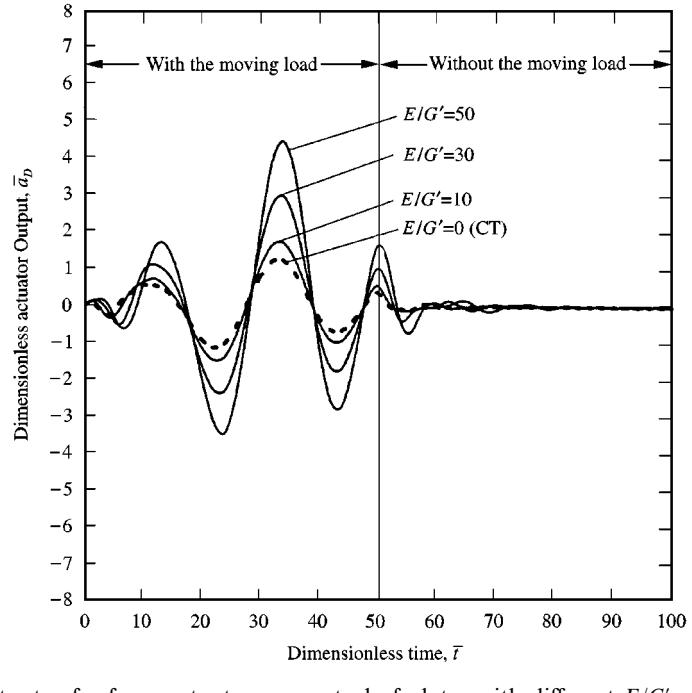

Figure 4. Outputs of a force actuator on control of plates with different E/G' ratios. CMC and IMSC, $\mathbf{R}_c = r_w \mathbf{B}_n^{*\mathrm{T}} \mathbf{B}_n^*$, $r_w = 10$, $q_w = 1$, nominal plant: CT, actual plant: HOT. In the remaining all the input data and convention are common to the ones in Figure 2.

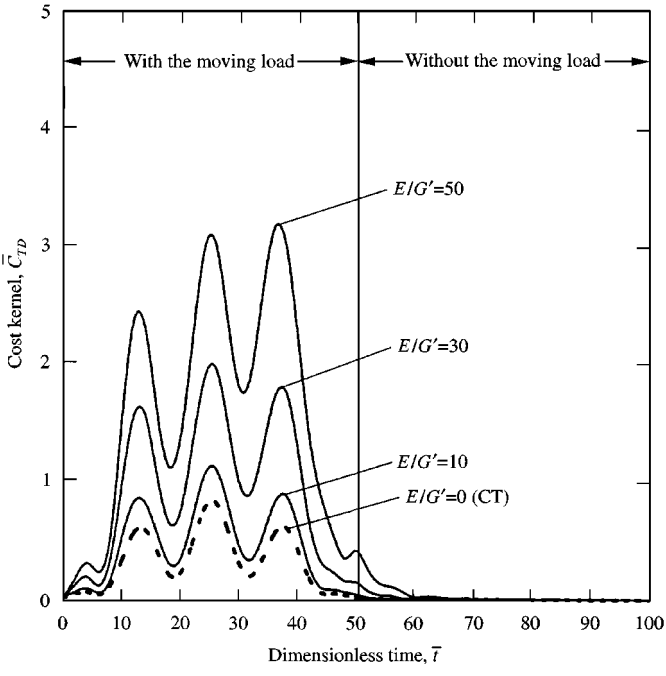

Figure 5. Cost kernels for control of plates featuring different E/G'. Others see Figure 4.

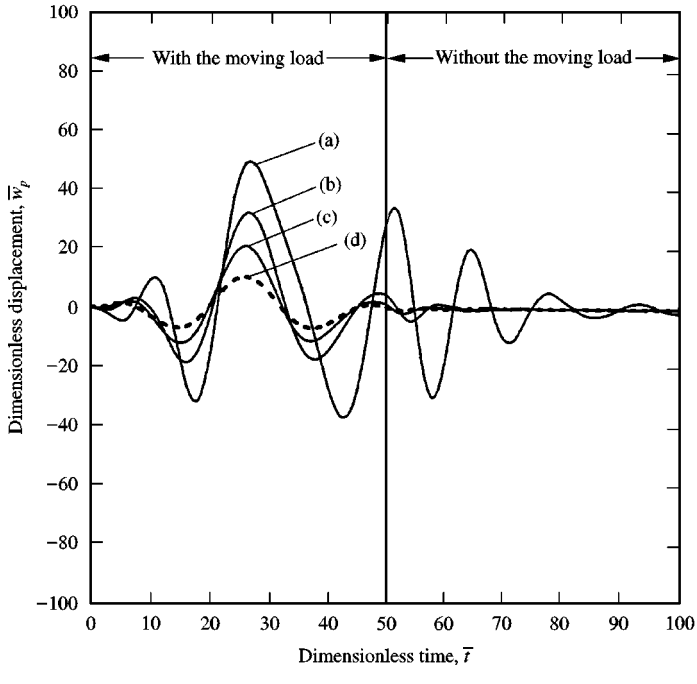

Figure 6. Controlled dimensionless transverse deflections of initially stressed plates. CMC and IMSC, $\mathbf{R}_c = r_w \mathbf{B}_n^{*T} \mathbf{B}_n^*$, $r_w = 10$, $q_w = 1$, $\bar{T}_2 = 0$, nominal plant: CT, $\bar{T}_1 = 0$. In the remaining all the input data and convention are common to the ones in Figure 2. Actual plant is (a) HOT, $\bar{T}_1 = -8$, (b) HOT, $\bar{T}_1 = 0$, (c) HOT, $\bar{T}_1 = 10$, (d) CT, $\bar{T}_1 = 0$.

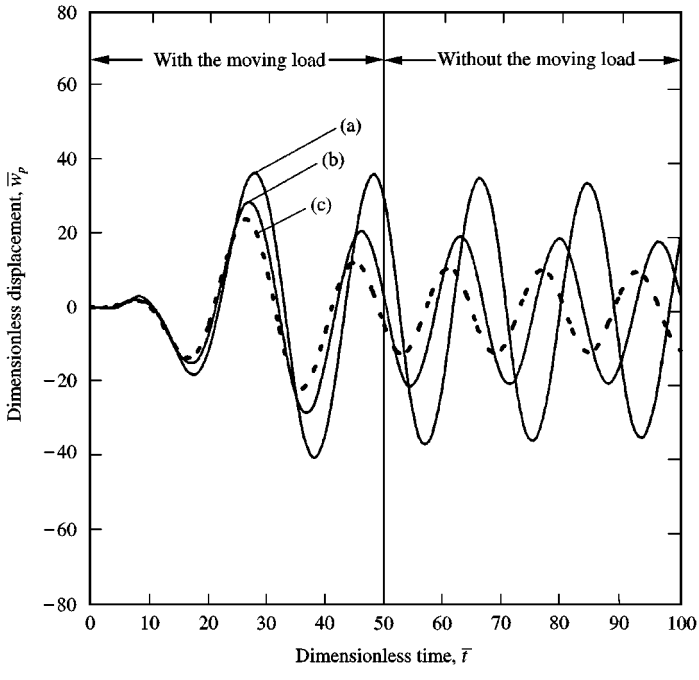

Figure 7. Uncontrolled dimensionless transverse deflections of laminates. $\ell_1/h = 20$, $\ell_R = 0{\cdot}75$, $\bar{v} = 0{\cdot}02$, $\bar{T}_1 = \bar{T}_2 = 0$, $\xi = 0{\cdot}005$, $\bar{\omega} = 0{\cdot}25$, (a) laminate B, HOT, (b) laminate A, HOT, (c) laminates A and B, CT.

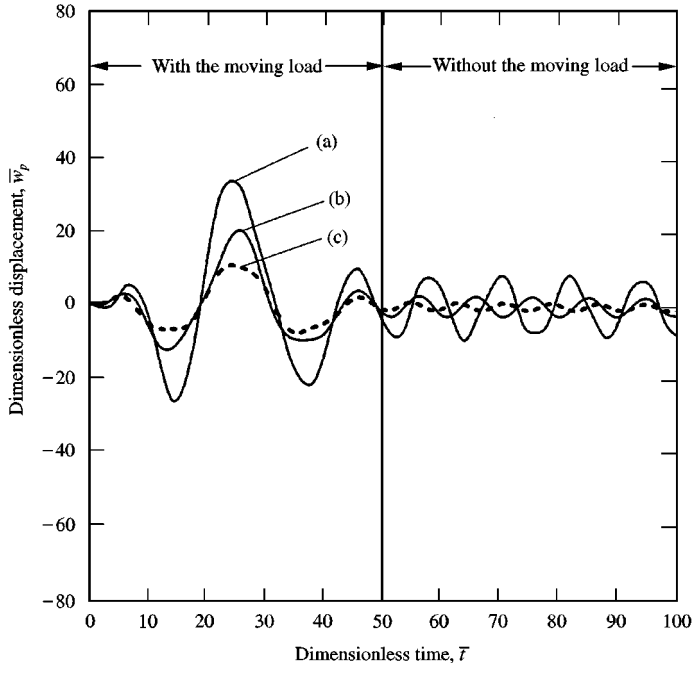

Figure 8. Uncontrolled dimensionless transverse deflections of laminates. $\ell_1/h = 10$; others, see Figure 7.

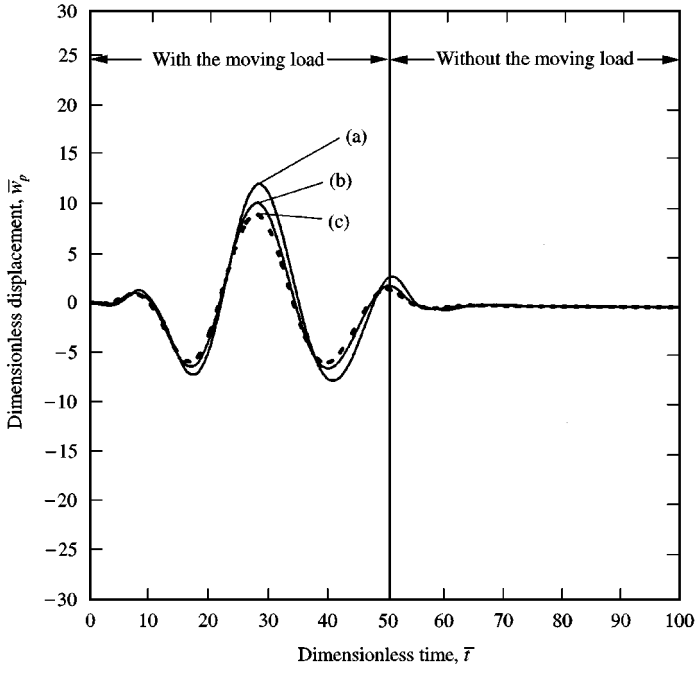

Figure 9. Controlled dimensionless transverse deflections of laminates. $\ell_1/h = 20$, $\ell_R = 0{\cdot}75$, $\bar{v} = 0{\cdot}02$, $\bar{T}_1 = \bar{T}_2 = 0$, $\xi = 0{\cdot}005$, $\bar{\omega} = 0{\cdot}25$, CMC and IMSC, $\mathbf{R}_c = r_w \mathbf{B}_n^{*\mathrm{T}} \mathbf{B}_n^*$, $r_w = 10$, $q_w = 1$, nominal plant: CT, actual plant is (a) laminate B, HOT, (b) laminate A, HOT, (c) laminates A and B, CT.

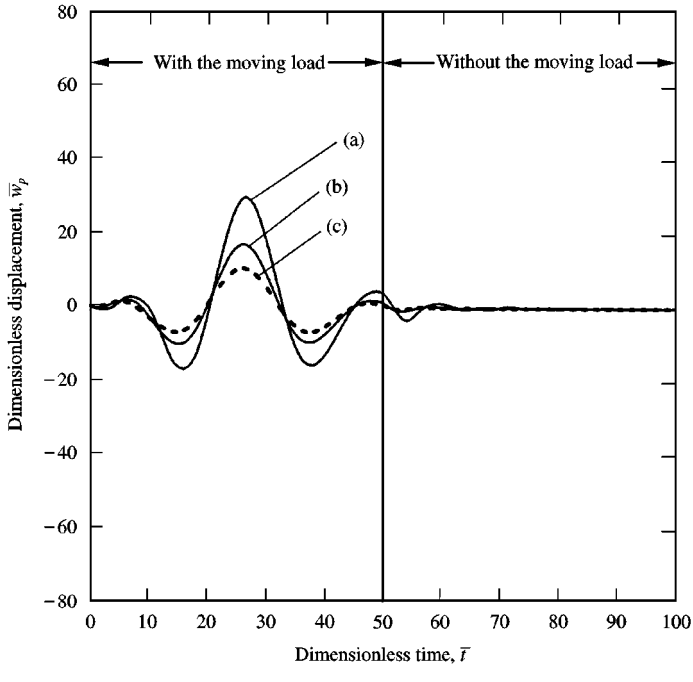

Figure 10. Controlled dimensionless transverse deflections of laminates. $\ell_1/h = 10$; others, see Figure 9.

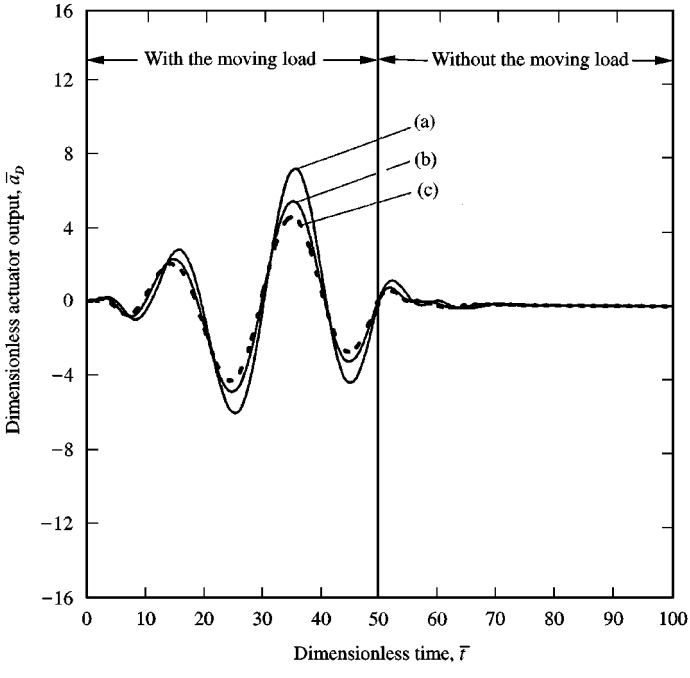

Figure 11. Comparison of the outputs of a force actuator on control of laminates A and B. $\ell_1/h = 20$; others, see Figure 9.

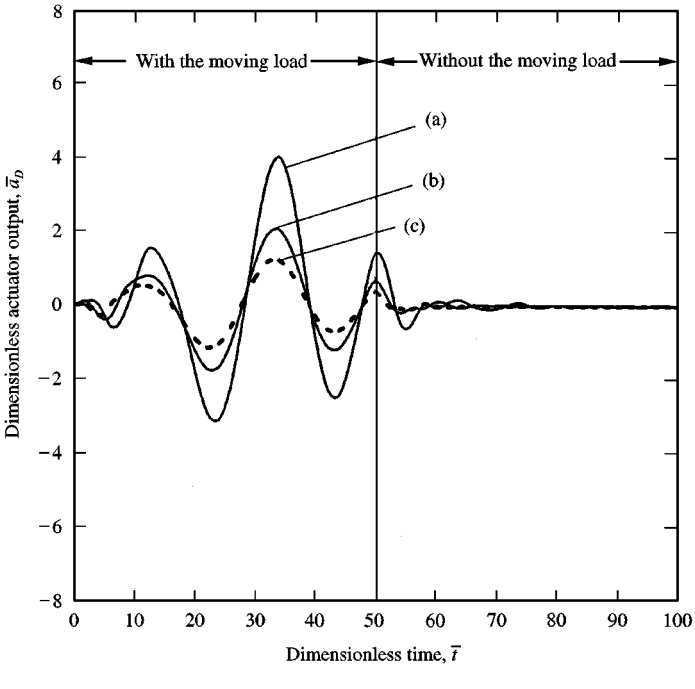

Figure 12. Comparison of the outputs of a force actuator on control of laminates A and B. $\ell_1/h = 10$; others, see Figure 9.

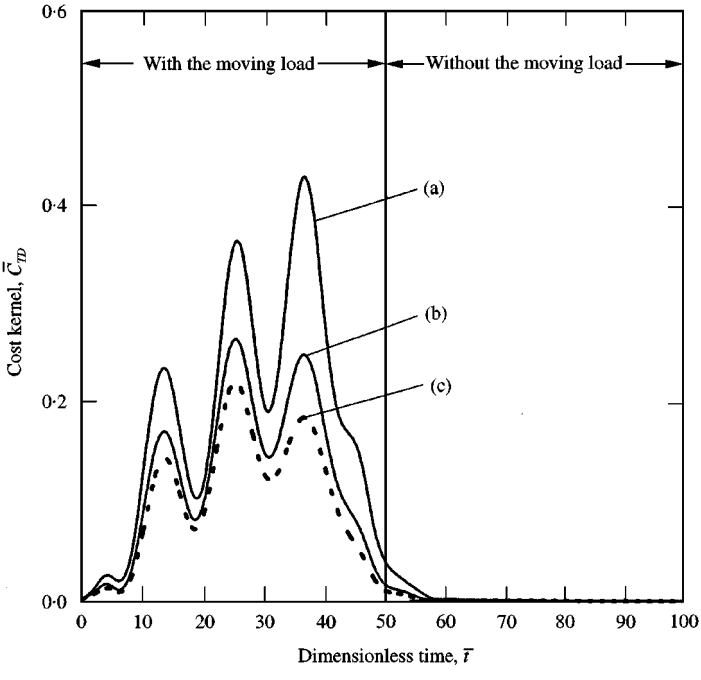

Figure 13. Cost kernels for control of laminates A and B. $\ell_1/h = 20$; others, see Figure 9.

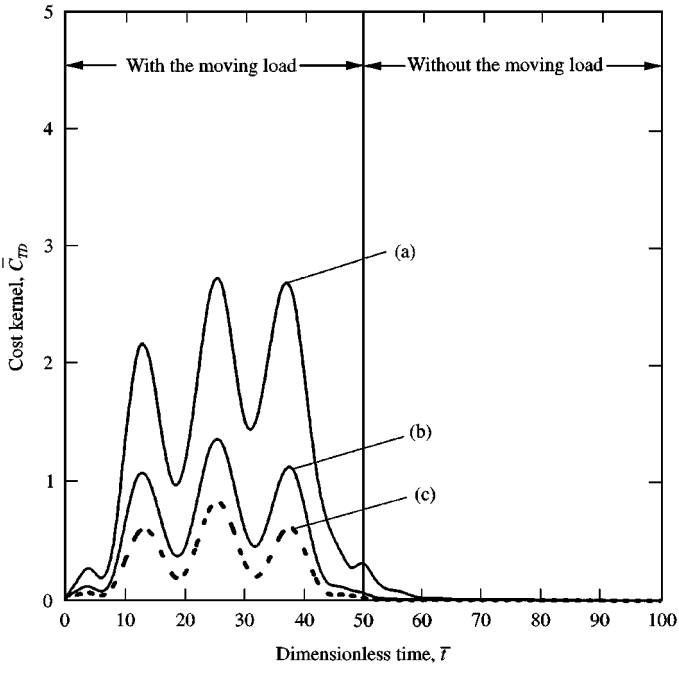

Figure 14. Cost kernels for control of laminates A and B. $\ell_1/h = 10$; others, see Figure 9.

Figures 9 and 10, the controlled deflections predicted by HOT and CT for laminates A and B are shown. For $\ell_1/h = 20$ case, as shown in Figure 9, the difference of the controlled deflections between laminates A and B, as well as between CT and HOT is less conspicuous. However, for thicker plates, the difference becomes noticeable as shown in Figure 10. The outputs of the first force actuator of the group 1 for the controlled systems in Figures 9 and 10 are shown in Figures 11 and 12 respectively. A large difference between the amplitudes of the actuator's output obtained from CT and HOT for the case of thicker laminate is found. This gives us a warning that when the plate modelled in the context of CT is used to design controller, one might face the possibility of the saturation of the actuators. If this happens, the controlled system's performance will certainly degrade further.

In Figures 13 and 14, the influence of the ℓ_1/h ratios on the cost kernels of laminates A and B is demonstrated. It reveals that larger cost kernels are required in the case of thicker panels and of laminated structures featuring larger transverse shear flexibility in the face layers, than in the core layer. Moreover, the results already obtained namely the underestimation of the cost kernel by the nominal plant, appears also in this case, and is shown to be even exacerbated for moderately thick panels.

Next, a second set of actuators (group 2) is chosen to control the plate described in Figure 2, and the results are given in Figures 15–17. In Figure 15 it is found that if a controller is designed based on a plate model of CT (which is used as the nominal plant) and is used to control a plate model of either FOT or HOT (simulated as the actual plant), the controlled systems become unstable. However, if both actual and nominal plants are modelled by CT, it is found that the response remains bounded (i.e., the controlled system is stable). For the purpose of comparison, the case with both nominal and actual plants simulated by plate model of HOT is also given. As is expected, in this case the controlled system is stable.

The results shown in Figure 15 apply to both IMSC and CMC approaches because the weighting matrix for control inputs of the form $\mathbf{R}_c = \mathbf{B}_n^{*\mathrm{T}}\mathbf{R}_I\mathbf{B}_n^*$ is used in the above example (see reference [10]). The natural frequencies of the plate and the closed-loop poles of the unstable controlled system are listed in Table 1 for reference.

It is evident from the results of the examples given above that the occurrence of unstable controlled systems in Figure 15 could be caused by the interplay of the following factors. The first factor is the modelling error. Here, it is due to the difference between the CT plate model being used in the design of the controller and the actual plant (here it is modelled using either HOT or FOT) to which the controller actually applies. The second one is the locations of actuators, which may be improperly chosen in contrast with those of the actuators of group 1. The third is the weighting matrix $\mathbf{R}_c$ selected in the design of the controller. It depends on the structural properties of the plate and therefore will be affected by the plate model being used. The influence of the last factor is illustrated in the following examples.

In Figure 16, the control input weighting matrix used in Figure 15 is changed into $\mathbf{R}_c = r_w\mathbf{I}$, where $r_w = 0{\cdot}001$. Hence, the weighting matrices being used now are all independent of structural properties. The nominal plant is still modelled by CT,

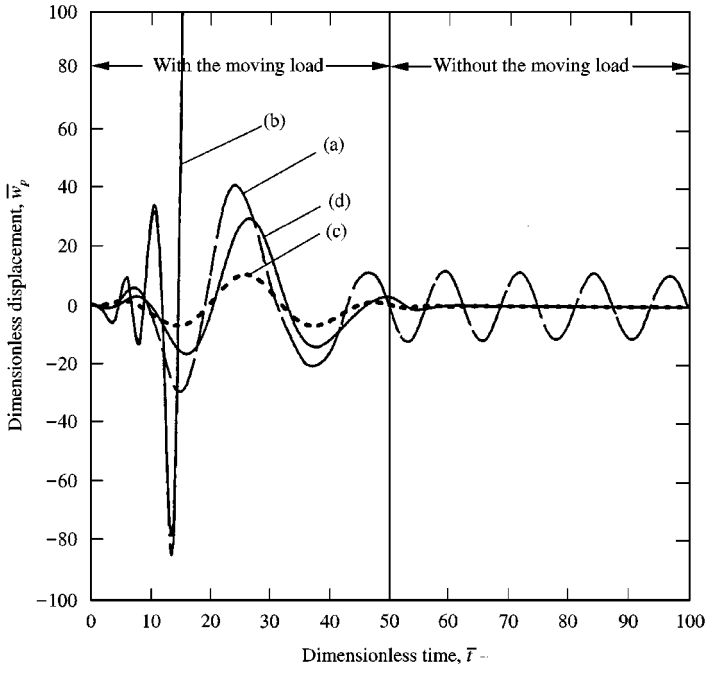

Figure 15. Controlled and uncontrolled dimensionless transverse deflections of a plate predicted by various plate models. CMC and IMSC, $\mathbf{R}_c = r_w \mathbf{B}_n^{*\mathrm{T}} \mathbf{B}_n^*$, $r_w = 10$, $q_w = 1$, 9 actuators (group 2). In the remaining all the input data and convention are common to the ones in Figures 2. (a) uncontrolled (HOT), (b) nominal plant: CT, actual plant: HOT & FOT, (c) nominal and actual plants: CT, (d) nominal and actual plants: HOT.

TABLE 1

Closed-loop poles of the unstable actively controlled plates

Mode number (m, n)	Natural frequency (HOT)	Closed-loop poles nominal plant : CT actual plant: HOT
(1, 1)	0·5052	− 0·4049 ± 0·3331
(1, 2)	1·009	− 0·2266 ± 0·9982
(1, 3)	1·539	− 0·02855 ± 1·499
(2, 1)	0·8205	− 0·08814 ± 0·8329
(2, 2)	1·212	**0·3636 ± 1·289**
(2, 3)	1·682	− 0·05727 ± 1·683
(3, 1)	1·191	− 0·1497 ± 1·224
(3, 2)	1·494	− 0·08281 ± 1·495
(3, 3)	1·897	− 0·2007 ± 1·973

while other conditions remain the same as those in Figure 15. As a result, the controlled responses now are all bounded. This indicates that the weighting matrix does play an important role of causing some controlled systems in Figure 15 to become unstable. In Figures 17 and 18, respectively, the influences of the control

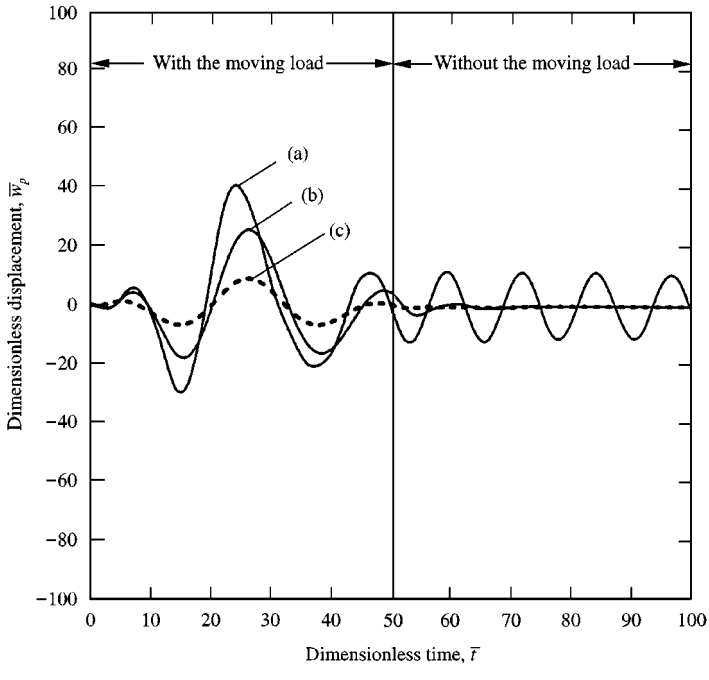

Figure 16. Controlled and uncontrolled dimensionless transverse deflections of a plate predicted by various plate models. CMC, $\mathbf{R}_c = r_w\mathbf{I}$, $r_w = 0{\cdot}001$, $q_w = 1$. In the remaining all the input data and convention are common to the ones in Figures 2. Nominal plant: CT, (a) uncontrolled (HOT), (b) actual plant: HOT, (c) actual plant: CT.

input weighting parameter r_w and the E/G' ratios on the closed-loop poles of the unstable system, where the actual plant is modelled using HOT in Figure 15, are illustrated. It is found that as r_w decreases (which amounts to larger control inputs are exerted) or E/G' ratio increases, one pair of unstable closed-loop poles appears and is driven further into the right-half plane. Hence for plates with large E/G' ratio, care should be taken not to adopt the vibration controller designed based on the plate model of CT. In Figure 18, the ninth pair of closed-loop poles is omitted for the sake of clarity.

6. CONCLUSIONS

A formulation for vibration control of composite laminated plates using the modal control approach is developed in this paper. Two different plate models based on the classical and a higher order plate theory are used to evaluate the influence of structural modelling effects on the effectiveness of the active control. By comparing the controlled response of the plate modelled by these two theories, the inadvertent predictions provided by the classical plate model on the vibration controller design were clearly indicated. As shown in numerical examples, the true controlled responses, cost kernels and actuators' outputs provided by a theory incorporating the non-classical structural effects can be inadvertently underestimated by using the control system based on the classical structural model.

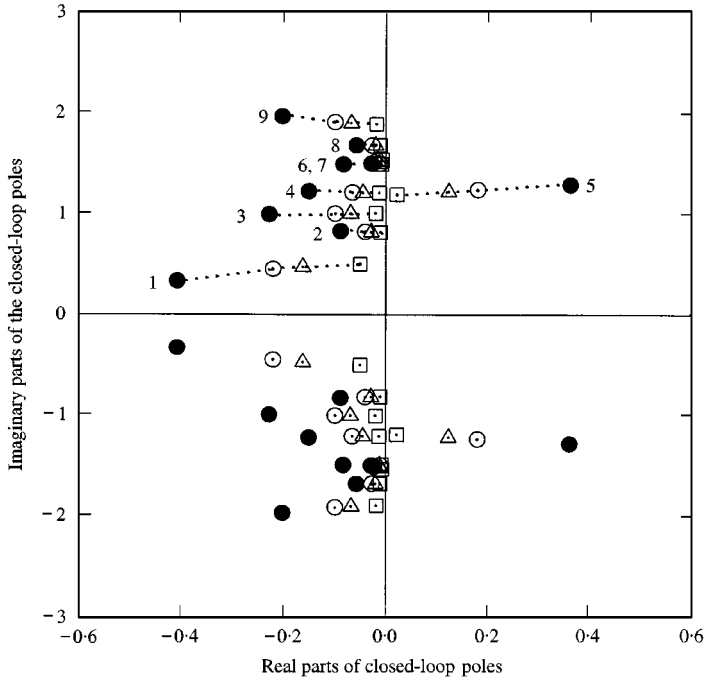

Figure 17. Variations of closed-loop poles of the unstable controlled system with control input weighting parameter, r_w. Actual plant: HOT, others, see Figure 15. ● $r_w = 10$; ⊙ $r_w = 50$; △ $r_w = 100$; ⊡ $r_w = 1000$.

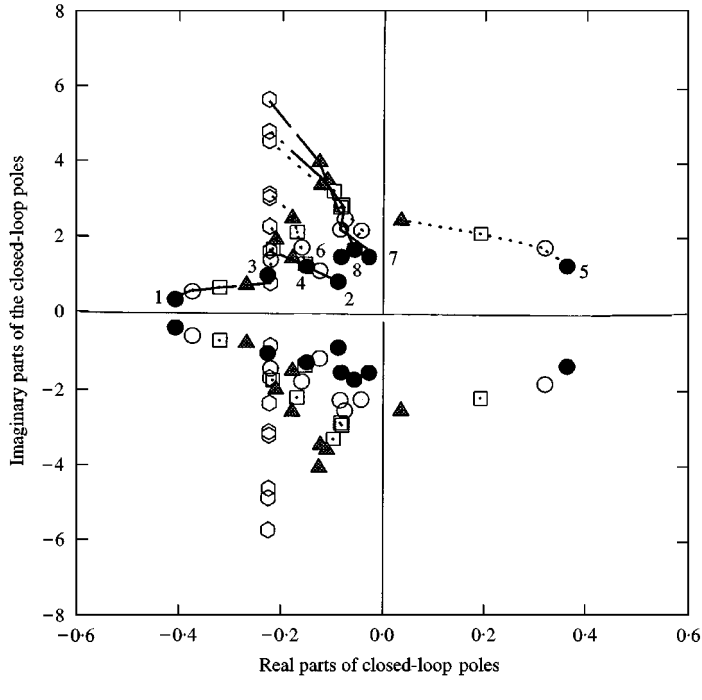

Figure 18. Variations of the closed-loop poles of the unstable controlled systems with E/G' ratios. ● $E/G' = 50$; ○ $E/G' = 20$; ⊡ $E/G' = 10$; ▲ $E/G' = 5$; ⬡ $E/G' = 0$.

Sometimes this could even lead to instability of the controlled system. Moreover, the results also reveal that when the classical plate theory is used to model the plant, the controlled response characteristics are *indifferent* to any variation of transverse shear flexibility featured by the material of the plant.

This implies that in order to achieve a reliable active control of structural systems constructed of advanced composite materials, transverse shear flexibility featured by the actual constituent materials has to be necessarily incorporated in the structural model.

REFERENCES

1. L. Meirovitch 1990 *Dynamics and Control of Structures*. New York: Wiley.
2. J. E. Lagnese and J.-L. Lions 1988 *Modelling Analysis and Control of Thin Plate*. Paris: Masson.
3. J. E. Lagnese 1989 *Studies in Applied Mathematics*, Vol. 10, Philadelphia, PA: SIAM Publ., Boundary stabilization of thin plates.
4. S. Adali, J. S. Sadek, J. M. Sloss and J. C. Bruch Jr. 1988 *Optimal Control Applications and Methods* **9**, 1–17. Distributed control of layered orthotropic plates with damping.
5. J. M. Sloss, J. S. Sadek, J. C. Bruch Jr. and S. Adali 1989 *IMA Journal of Mathematical Control and Information* **6**, 217–232. Applications of maximum principle for the structural control of laminated composite plates.
6. S. Adali, J. C. Bruch Jr. J. S. Sadek and J. M. Sloss 1992 *Journal of Sound and Vibration* **156**, 207–216. Energy minimization of vibrating plates subject to constraints on open and closed loop control forces.
7. L. Librescu 1975 *Elastostatics and Kinetics of Anisotropic and Heterogeneous Shell-Type Structures*. The Netherlands: Sijthhoff & Noordhoff.
8. L. Librescu and J. N. Reddy 1989 *International Journal of Engineer Science* **27**, 515–527. A few remarks concerning several refined theories of anisotropic composite laminated plates.
9. K. M. Liew, Y. Xiang and S. Kitipornchai 1995 *Journal of Sound and Vibration* **180**, 163–176. Research on thick plate vibration: a literature survey.
10. L. Meirovitch, H. Baruch and H. Öz 1983 *Journal of Guidance, Control, Dynamics* **6**, 302–310. A comparison of control technique for large flexible systems.
11. D. E. Kirk 1970 *Optimal Control Theory An Introduction*. NJ: Prentice-Hall, Englewood Cliffs.
12. L. Librescu and M. Stein 1991 *Thin-Walled Structures* **11**, 177–201. A Geometrically nonlinear theory of transversely isotropic laminated composite plates and its use in the post-buckling analysis.
13. M. J. Balas 1978 *Journal of Optimization theory and Applications* **25**, 415–436. Active control of flexible systems.

APPENDIX: NOMENCLATURE

$\tilde{a}_i$	amplitudes of control forces
$\mathbf{A}_N$, $\mathbf{A}$, $\mathbf{A}_{ij}$	system matrices
$\mathbf{A}_N^*$	closed-loop system matrix
$\mathbf{B}_N$, $\mathbf{B}$, $\mathbf{b}_c$	input matrices
C_T	cost kernel
$diag\{\ \}$	the diagonal matrix
$E_{(r)}$, $E'_{(r)}$	Young's moduli of the rth layer associated with the isotropy plane and the planes normal to the isotropy plane respectively

f_{dij}, f_{cij} modal external and control forces respectively
$\mathbf{f}_d$ external modal force vector
$G_{(r)}, G'_{(r)}$ shear moduli of the rth layer associated with the isotropy plane and the planes normal to the isotropy plane respectively
h total thickness of the plate
J cost function
ℓ_1, ℓ_2 dimensions of rectangular plate in the x- and y-axis directions respectively
$\ell_R (\equiv \ell_2/\ell_1)$ plate aspect ratio
$\mathbf{M}$ transformation matrix whose columns consists of the eigenvectors of $\mathbf{A}_N^*$
m_1, m_2 external moment intensities with their applied axes parallel to the x-axis and y-axis respectively
$\tilde{m}_{1j}, \tilde{m}_{2j}$ amplitudes of control moments
N_{ij} generalized masses
p, p_c external transverse load intensity and control force
p_0, v, ω the amplitude, constant moving speed and frequency of the travelling oscillating force
$q_{ij}, \dot{q}_{ij}$ modal co-ordinates (or generalized co-ordinates) and modal velocities
q_{wij} state weighting parameters
$\mathbf{Q}, \mathbf{Q}_{ij}$ weighting matrices for states
$r_{wij} (\equiv r_w)$ control input weighting parameters
$\mathbf{R}, \mathbf{R}_c, \mathbf{R}_I$ weighting matrices for control inputs
$\mathbf{S}$ weighting matrix for terminal state vector $\mathbf{u}(t_f)$
t_0, t_f initial and terminal time of the intended controlling period
T_x, T_y the in-plane edge loads applied parallel to the x- and y-axis, respectively (positive in tension)
$T_R (\equiv T_2/T_1)$ tensile edge load ratio
$\mathbf{u}_N, \mathbf{u}, \mathbf{v}_{ij}$ state vectors consist of modal co-ordinates and modal velocities
w transverse plate displacement
$\mathbf{z}$ control input vector consists of $\tilde{a}_i, \tilde{m}_{1j}, \tilde{m}_{2j}$
β_α rotations of the deformed normal
δ_A tracer identifying the transverse normal stress (i.e. σ_{zz}) effect
Φ transverse shear potential function
ϕ_{ij} normalized eigenfunctions
ξ_{ij} damping ratios
λ_i eigenvalues of A_N^*
$\mu_{(r)}, \mu'_{(r)}$ the Poisson ratios of the rth layer associated with the isotropy plane and the planes normal to the isotropy plane respectively
$\rho_{(r)}$ mass density of the rth layer
Ω_{ij} eigenfrequencies (i.e., natural frequencies)
ψ_α higher order in-plane displacement functions accounting for deformation of the originally flat cross-section

APPENDIX B

Mass and rigidity coefficients:

$$K = M_0\left[\frac{B+C}{S} + \delta_A\left(\frac{F}{M_0} - \frac{L}{S}\right)\right], \qquad H_1 = \frac{B+C}{S} - \delta_A\frac{L}{S},$$

$$H_2 = \frac{1}{6}\left(\frac{B+C}{S} - \delta_A\frac{2L}{S}\right),$$

$$M_0 = 2\left[\rho_{(m+1)}h_{(m+1)} + \sum_{r=1}^{m}\rho_{(r)}(h_{(r)} - h_{(r+1)})\right],$$

$$B = \frac{1}{3}\left[\tilde{E}_{(m+1)}(1+\mu_{(m+1)})h^3_{(m+1)} + \sum_{r=1}^{m}\tilde{E}_{(r)}(1+\mu_{(r)})(h^3_{(r)} - h^3_{(r+1)})\right]$$
$$- \frac{4}{15h^2}\left[\tilde{E}_{(m+1)}(1+\mu_{(m+1)})h^5_{(m+1)} + \sum_{r=1}^{m}\tilde{E}_{(r)}(1+\mu_{(r)})(h^5_{(r)} - h^5_{(r+1)})\right],$$

$$C = \frac{1}{3}\left[\tilde{E}_{(m+1)}(1-\mu_{(m+1)})h^3_{(m+1)} + \sum_{r=1}^{m}\tilde{E}_{(r)}(1-\mu_{(r)})(h^3_{(r)} - h^3_{(r+1)})\right]$$
$$- \frac{4}{15h^2}\left[\tilde{E}_{(m+1)}(1-\mu_{(m+1)})h^5_{(m+1)} + \sum_{r=1}^{m}\tilde{E}_{(r)}(1-\mu_{(r)})(h^5_{(r)} - h^5_{(r+1)})\right],$$

$$D = \frac{2}{3}\left[\tilde{E}_{(m+1)}h^3_{(m+1)} + \sum_{r=1}^{m}\tilde{E}_{(r)}(h^3_{(r)} - h^3_{(r+1)})\right],$$

$$S = 2G'_{(m+1)}h_{(m+1)} + 2\sum_{r=1}^{m}G'_{(r)}(h_{(r)} - h_{(r+1)})$$
$$- \frac{8}{3h^2}\left[G'_{(m+1)}h^3_{(m+1)} + \sum_{r=1}^{m}G'_{(r)}(h^3_{(r)} - h^3_{(r+1)})\right],$$

$$L = \frac{2}{3}\left[\frac{\mu'_{(m+1)}E_{(m+1)}G'_{(m+1)}}{E'_{(m+1)}(1-\mu_{(m+1)})}h^3_{(m+1)} + \sum_{r=1}^{m}\frac{\mu'_{(r)}E_{(r)}G'_{(r)}}{E'_{(r)}(1-\mu_{(r)})}(h^3_{(r)} - h^3_{(r+1)})\right.$$
$$\left. - \frac{4}{5h^2}\frac{\mu'_{(m+1)}E_{(m+1)}G'_{(m+1)}}{E'_{(m+1)}(1-\mu_{(m+1)})}h^5_{(m+1)} + \sum_{r=1}^{m}\frac{\mu'_{(r)}E_{(r)}G'_{(r)}}{E'_{(r)}(1-\mu_{(r)})}(h^5_{(r)} - h^5_{(r+1)})\right],$$

$$F = \frac{2}{3}\left[\frac{E_{(m+1)}\mu'_{(m+1)}}{E'_{(m+1)}(1-\mu_{(m+1)})}\rho_{(m+1)}h^3_{(m+1)} + \sum_{r=1}^{m}\frac{E_{(r)}\mu'_{(r)}}{E'_{(r)}(1-\mu_{(r)})}\rho_{(r)}(h^3_{(r)} - h^3_{(r+1)})\right].$$

Here

$$\tilde{E} \equiv E/(1-\mu^2).$$

APPENDIX C

Dimensionless parameters:

$$\bar{x} = \frac{x}{\ell_1}, \qquad \bar{y} = \frac{y}{\ell_2}, \qquad \bar{w} = \frac{w}{h}, \qquad \bar{R} = \frac{C}{S\ell_2^2}, \qquad \bar{B} = 12\,\frac{\ell_1}{h}\,(\ell_R)^2,$$

$$\bar{C}_1 = 12(\ell_R)^2\,\frac{C}{h^2(B+C)}, \quad \bar{C}_2 = \bar{C}_1\frac{1}{(\ell_R)^2}, \quad \bar{\Phi} = \frac{\ell_1^3\Phi}{h\ell_2 D}, \quad \bar{T}_1 = T_x\frac{\ell_2^2}{D},$$

$$\bar{T} = T_y \frac{\ell_1^2}{D}, \quad \bar{D}_1 = (\ell_R)^2, \quad \bar{D}_2 = \frac{1}{\bar{D}_1}, \quad \bar{F}_1 = \frac{H_1}{\ell_1^2}, \quad \bar{F}_2 = \frac{H_1}{\ell_2^2}, \quad \bar{p} = \frac{\ell_1^2 \ell_2^2}{Dh}\, p,$$

$$\bar{t} = \frac{t}{\ell_1 h}\sqrt{\frac{12D}{(B+C)}}, \quad \bar{\Omega} = \Omega \ell_1 h \sqrt{\frac{(B+C)}{12D}}, \quad \bar{a}_D = \frac{10\tilde{a}}{p_0}, \quad \bar{C}_{TD} = \frac{10^5 (Dh)^2}{(p_0 \ell_1 \ell_2)^2}\, \bar{C}_T,$$

$$\bar{p}_0 = p_0 \frac{\ell_1 \ell_2}{Dh}, \quad \bar{v} = vh\sqrt{\frac{(B+C)}{12D}}, \quad \bar{\omega} = \omega h \ell_1 \sqrt{\frac{(B+C)}{12D}}, \quad \bar{\delta}(\bar{x}) = \ell_1 \delta(x),$$

$$\bar{\delta}(\bar{y}) = \ell_2 \delta(y), \quad \bar{w}_p = \frac{10^3 Dh}{p_0 \ell_1 \ell_2}\, \bar{w}, \quad \bar{F}_{11} = \frac{H_2}{\ell_1^2}, \quad \bar{F}_{12} = \frac{H_2}{\ell_2^2},$$

$$\bar{m}_1 = m_1 \frac{\ell_1^2 \ell_2}{Dh}, \qquad \bar{m}_2 = m_2 \frac{\ell_2^2 \ell_1}{Dh}.$$